Singlet Fission and Triplet Exciton Dynamics in Rubrene/Fullerene Heterojunctions: Implications for Electroluminescence

ARTICLE · NOVEMBER 2015

DOI: 10.1002/aelm.201500229

5 AUTHORS, INCLUDING:

Mujeeb Ullah

University of Queensland

44 PUBLICATIONS **513** CITATIONS

SEE PROFILE

Soniya D. Yambem

Queensland University of Technology

22 PUBLICATIONS **166** CITATIONS

SEE PROFILE

Ajay K. Pandey

Queensland University of Technology

44 PUBLICATIONS **778** CITATIONS

SEE PROFILE

ADVANCED ELECTRONIC MATERIALS
www.advelectronicmat.de

Singlet Fission and Triplet Exciton Dynamics in Rubrene/Fullerene Heterojunctions: Implications for Electroluminescence

*Mujeeb Ullah, Soniya D. Yambem, Evan G. Moore, Ebinazar B. Namdas, and Ajay K. Pandey**

The role of triplet excitons in rubrene/C_{60} heterojunctions is investigated through detailed spectroscopic studies of triplet generation routes in the neat and heterojunction films of rubrene and C_{60}. Time-correlated single-photon counting experiments on rubrene and rubrene/C_{60} give a long-lived component with lifetime >200 ns, and triplets are found to live longer in rubrene/C_{60}. A distinct reduction at short time scales in fluorescence lifetime of rubrene/C_{60} gives the indication of singlet exciton dissociation via formation of charge-transfer (CT) states. Using ultrafast transient absorption spectroscopy, it is found that triplets are generated via singlet-fission in neat rubrene films at $t \approx 1.8$ ps, whereas a delayed population buildup of triplets in rubrene/C_{60} occurs at $t \approx 8$ ps. The slow rise of triplet population confirms the role of CT-state-mediated triplet energy transfer in rubrene/C_{60}. The recombination of triplets via triplet–triplet annihilation in organic light-emitting diode (OLED) operation of rubrene/C_{60} is shown to generate extra singlets, which lift the spin branching ratio to values >25%. It is concluded that triplet excitons in rubrene/C_{60} are instrumental in bringing lower turn-on voltages, brighter emission, and higher external quantum efficiency of electroluminescence in OLED and light-emitting field effect transistors.

1. Introduction

Light emission under the application of an electric field is one of the fundamental properties of organic semiconductors, and the overall efficiency of light emission depends on charge balance in the device, the spin character of injected electron–hole pairs, and the solid state photoluminescence (PL) efficiency of the semiconducting material.[1–4] Equation (1) relates all factors that influence the external quantum efficiency (EQE) of light emission in organic semiconductors[4]

$$\varphi_{EQE} = \varphi_{capture} \times \varphi_{spin} \times \varphi_{PLQY} \times \varphi_{escape} \quad (1)$$

where $\varphi_{capture}$ is the fraction of electrons and holes that recombine to form excitons (recombination efficiency), φ_{EQE} is experimentally determined EQE, φ_{escape} is the fraction of photons that can escape from the device, φ_{spin} is the factor allowed due to spin statistics, and φ_{PLQY} is the photoluminescence quantum yield (PLQY) in the solid state. The percentage of photons that can escape from device, φ_{escape}, is $\approx 1/2n^2$ (where n is the refractive index of the organic layer).

In organic fluorescent emitters, the φ_{spin} limit is fixed at 25% due to the singlet–triplet branching ratio of 1:3. However, φ_{spin} limit has been extended to 100% in organic phosphorescent emitters using the metal–ligand-based spin–orbit coupling approach that allows efficient intersystem crossing in organic semiconductors.[1,3] On the other hand, in fluorescent emitters, mechanisms such as thermally assisted delayed fluorescence and triplet–triplet annihilation (TTA) are uniquely capable of enhancing φ_{spin} well above the classical limit of 25%.[5–7] Triplet exciton harvesting is expected to play an important role in closing the efficiency gap between phosphorescent and fluorescent emitters. Therefore, understanding triplet exciton dynamics in organic semiconductor heterojunctions is essential to overall efficient operation of organic optoelectronic devices.

Rubrene is a fluorescent emitter that is also known to undergo singlet fission, where a singlet exciton breaks into two low energy triplet excitons.[8–12] Under the isoergic case of singlet fission [$E(S_1) = 2E(T_1)$], where S_1 and T_1 are the singlet and triplet energies, the singlet fission process becomes reversible, which means generation of a high-energy singlet state through annihilation of two low energy triplets is possible.[9,12] In situations like this, two independent channels of charge injection and recombination via singlet and triplet states are accessible. Recently, we reported TTA as a highly efficient spin-conversion mechanism in rubrene/C_{60} heterojunctions.[10] In this model system, the TTA process induces an energy upconverted

Dr. M. Ullah, Dr. S. D. Yambem, Dr. E. B. Namdas, Dr. A. K. Pandey
Centre for Organic Photonics and Electronics
The University of Queensland
Brisbane 4072, QLD, Australia
E-mail: a2.pandey@qut.edu.au
Dr. E. G. Moore, Dr. A. K. Pandey
School of Chemistry and Molecular Biosciences
The University of Queensland
Brisbane 4072, QLD, Australia
Dr. A. K. Pandey
School of Electrical Engineering and Computer Science
Queensland University of Technology
Brisbane 4000 QLD, Australia

DOI: 10.1002/aelm.201500229

electroluminescence (UC-EL) effect, whereby orange light emission (EL peak at 570 nm) was observed at an extremely low driving voltage of +1 V. This observation has established the general role of triplet excitons in EL, and triplet exciton harvesting has been shown as the additional route for extra singlet generation in organic light-emitting diodes (OLEDs).

Assuming that two triplets successfully recombine to generate a singlet, the TTA event is capable of increasing the overall singlet generation yield of fluorescent emitters from 25% to up to 62.5% (25% + 75%/2 = 62.5%).[7] However, a selective assessment of TTA induced singlet emission from that of standard singlet states is not always straightforward and ascertaining the influence of TTA on EL in operational devices requires careful considerations of performance factors identified in Equation (1). An alternative way to confirm the influence of TTA is to monitor the recombination efficiency ($\varphi_{capture}$) component of Equation (1).

In this study, we set out to investigate: (i) singlet exciton fission and triplet exciton dynamics including TTA in rubrene/C_{60} heterojunction through detailed spectroscopic studies, and (ii) the influence of TTA on overall efficiency of light emission in OLEDs and light-emitting field effect transistors (LEFETs) that are composed of rubrene and rubrene/C_{60}. We show that the presence of C_{60} with rubrene leads to lower light turn-on voltages, brighter light emission, and higher EQEs in both LEFETs and OLEDs. The high EQE and low light turn-on voltage in the rubrene/C_{60} devices are consistent with TTA assisted recombination process identified by spectroscopic measurements.

2. Results and Discussion

2.1. Photoluminescence Kinetics and Ultrafast Transient Absorption Measurements

To achieve the above discussed objectives, we first probe the emission characteristics of thin films of rubrene and compare it with that from rubrene/C_{60} at the emission wavelength of 570 nm. **Figure 1** shows the PL decay over short (≈25 ns) as well as at long time scales (≈2 µs) of neat rubrene film measured in a nitrogen environment with an excitation wavelength of 470 nm using a time-correlated single-photon counting (TCSPC) setup. A triexponential fit to the PL decay curve of rubrene in Figure 1a gives a set of fast and slow components with values of 0.92 ns (64.2%), 2.93 ns (33.7%), and 25.0 ns (2.1%), where the values in the parenthesis represent the amplitude for each lifetime component. These results are in good agreement with values reported by Piland et al. and Ma et al., where authors reported multiexponential decays of fluorescence signal in amorphous and crystalline rubrene.[11,12] The PL decay measurements on rubrene/C_{60} sample shows an overall reduction in the PL lifetime of rubrene. The rubrene/C_{60} films give lifetimes of 0.53 ns (71.7%), 1.58 ns (27.3%), and 12.5 ns (2.1%). Here, a distinct reduction in fluorescence lifetime is a direct indication of PL quenching via CT states formed at the rubrene/C_{60} heterojunction. It is expected that the quenching of singlet emission of rubrene by C_{60} could play a significant role in the kinetics presented; therefore, we further verified PL

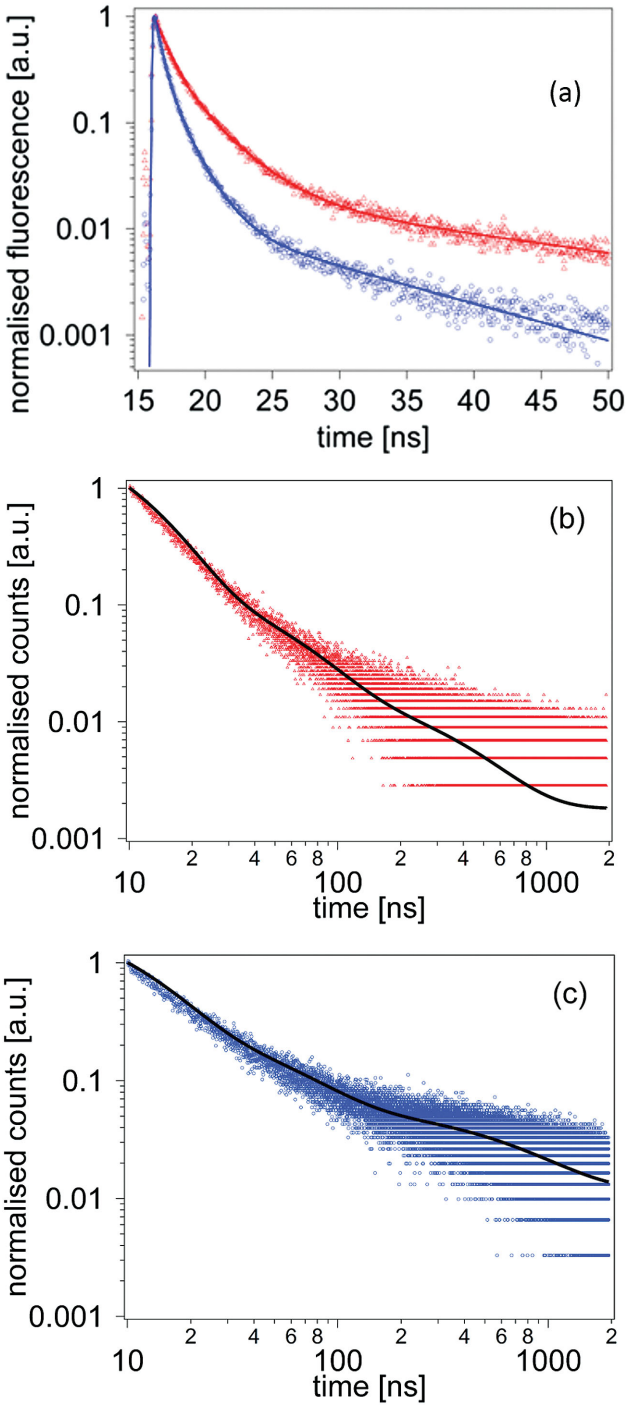

Figure 1. TCSPC results recorded at λ_{exc} = 350 nm. a) semilog plot comparing the PL decay at short time scales for rubrene (red curve) and rubrene/C_{60} (blue curve). The long-lived PL decay on log–log scale for b) rubrene and c) rubrene/C_{60} thin film is measured to ascertain the contribution of delayed PL originating from TTA event. The solid black line in each case represents a triexponential fit to the PL data.

quenching of rubrene by C_{60} in steady state PL measurements. Figure S1 (Supporting Information) presents the PL emission of rubrene, which is shown to quench by ≈50% in presence of C_{60}. The absorption spectra of rubrene, rubrene/C60, and C60

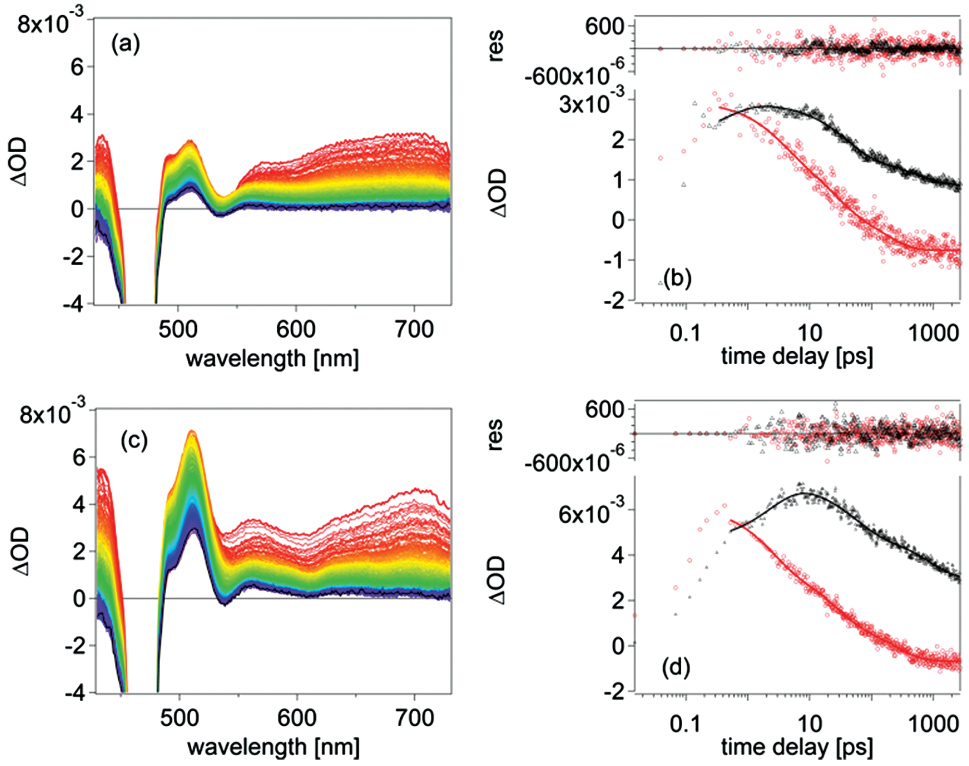

Figure 2. TA measurements on a) thin film of neat rubrene and b) kinetic traces of singlet and triplet peaks at 435 nm (red curve) and 510 nm (black curve), respectively for rubrene. c) TA spectra of rubrene/C_{60} thin film. d) Kinetic traces for singlet peak at 430 nm (red curve) and triplet peak at 510 nm of rubrene/C_{60} (black curve) are shown in (c,d).

thin films are presented in Figure S2 (Supporting Information). In addition, to PL quenching due to the absorption of C_{60} around 570 nm, it is plausible that some reabsorption of emission would reduce the PL signal. Under high excitation intensity significant amount of triplets can be generated.[13]

In order to probe the role of TTA in PL from rubrene and rubrene/C_{60} thin films, we measured the PL decay over a relatively longer time scale under very high excitation intensity (≈600 µW, 1 kHz, 0.6 µJ per pulse). Figure 1b (plotted on log–log scale) shows the long-lived tail of the PL decay for rubrene thin film that has a fitted lifetime of 279.1 ns. In Figure 1c, we show that under similar experimental conditions PL decay in rubrene/C_{60} film has an even longer lived lifetime component of 593.8 ns. The presence of long-lived component in PL is due to delayed PL emission via TTA event and triplets live longer in rubrene/C_{60} heterojunction than in pristine rubrene.

To further investigate the origin of long-lived triplets in rubrene/C_{60} over neat rubrene, we perform ultrafast transient absorption (TA) measurements on rubrene and rubrene/C_{60} thin films. **Figure 2**a presents the TA signals from rubrene thin film when photoexcited at 470 nm. The TA spectra show two distinct peaks. The peak at 435 nm is characteristic of $S_1 \rightarrow S_n$ absorption, whereas the peak at 510 nm is due to $T_1 \rightarrow T_n$ absorption and features from 550 to 700 nm are believed to arise from polarons in rubrene.[12] In addition, a small ground state bleach signal is also evident at 530 nm, although relatively weak bleaching of ground state indicates a higher oscillator strength for the $T_1 \rightarrow T_n$ absorption in rubrene. The kinetics for the singlet and triplet peaks of rubrene, as shown in Figure 2b, show a decay in the singlet population at 435 nm, followed by a rise in triplet population at 510 nm. Fit to the kinetics at 510 nm give a triplet population rise at ≈1.8 ps. This timescale is consistent with the thermally activated singlet fission character of rubrene.[12] Figure 2c shows the TA measurements on rubrene/C_{60} samples, and the corresponding kinetics are shown in Figure 2d. Although there is no change in the excited state absorption peak positions, there are significant changes in the time scale of triplet-population buildup. Unlike the almost instantaneous population build of triplets in neat rubrene at 1.8 ps, the triplet-population buildup in rubrene/C_{60} shows a slow rise that peaks at 8 ps. The two different timescales associated with triplet-population buildup suggest triplet generation via an additional route other than the singlet fission process in neat rubrene. For completeness, the TA spectra for thin films of neat C_{60} were also recorded with excitation at 470 nm (Figure S3 in the Supporting Information). The TA spectra of C_{60} have a peak at ≈530 nm, which decays quickly (≈1 ps). Nevertheless, the long wavelength features of C_{60} TA spectra are retained in rubrene/C_{60} films.

As established by Ma et al., triplet excitons in rubrene are formed via fission of the upper singlet states (within 200 fs) as well as from the lowest excited singlet state (picosecond time scale).[12] The ultrafast timescale of triplet formation from upper excited singlet state in rubrene would mean that quenching of the singlet via charge transfer to C_{60} proceeds only through the lowest exited singlet state. So, in the presence

of C_{60}, a reduction in singlet exciton by quenching would perturb just one channel of triplet formation. In fact, in our recent photovoltaic studies on rubrene/C_{60}, we have unequivocally shown that the energetics of rubrene/C_{60} heterojunction are as such that initial quenching of the lowest excited singlet exciton through charge transfer to C_{60} works as a triplet population channel through resonant coupling of the ^{3}CT state with the T1 state of rubrene.[10] With C_{60}, under high carrier concentrations, the quenching of singlet excitons at picosecond would end up increasing the overall triplet population in rubrene. We note that due to the lack of free energy at the rubrene/C_{60} interface the quenching of triplet excitons is not possible with C_{60}.[10] Therefore, the 1–10 ps plateau is an indication of triplet formation via fission of upper excited singlet states; the rise in the TA signal with a peak at ≈10 ps is a clear validation of the arrival of triplets through a charge transfer route.

We assign the slow buildup of the triplet level to the triplet energy transfer (TET) from C_{60} to rubrene via CT states. This is in good agreement with the PL decay of rubrene/C_{60} where triplets live longer than in neat rubrene. Furthermore, we find the evidence of excitation transfer from C_{60} to rubrene via TET in operational photovoltaic devices by probing the photocurrent generation at high carrier concentration. Figure S4 (Supporting Information) captures the back transfer of excitation to rubrene T1 via formation of ^{3}CT states. By identifying the two routes of triplet population in rubrene/C_{60} thin films, we next look at its influence on EL in OLED and LEFET devices.

2.2. Recombination Efficiency in Rubrene, and Rubrene/C_{60} Light-Emitting Diodes and EL Turn-On Below Subgap Voltages

Figure 3a shows the device architecture of rubrene/C_{60} heterojunction OLEDs. The rubrene control OLED was of similar structure. Like the samples used in PL and TA studies, the OLED device uses a 35 nm thin layer of rubrene and 25 nm of C_{60}. The current density–luminescence–voltage (*J–L–V*) characteristics of the OLEDs are shown in Figure 3b. The turn-on voltage for the control rubrene OLED was at 2 V. Figure 3c compares the EQE of light emission from rubrene/C_{60} and rubrene control with respect to brightness. The control device delivers a maximum brightness of 40 cd m^{-2} with an EQE of 4 × 10^{-4}%. In contrast, the rubrene/C_{60} heterojunction OLED shows much lower light turn-on voltage (≈1 V), and higher EQE (4.5 × 10^{-2}% at 1450 cd m^{-2}) than the control OLED. These results are consistent with energy UC-EL process in rubrene/C_{60} OLEDs.[10,14] We note that the observed turn-on voltage at 1 V for rubrene/C_{60} is much lower than the optical gap of rubrene (2.2 eV) and it rather correlates well with the triplet energy level (T1 = 1.12 eV) of rubrene. Based on the PL and TA measurements, we confer that TTA process to be rather efficient in rubrene/C_{60} OLEDs and the UC-EL arises from the annihilation of two triplet excitons in rubrene.[15]

Assuming a spin branching ratio of 25%, PLQY of 1.5% ± 0.2% and φ_{escape} ≈ 20%, we estimate the recombination efficiency for rubrene control to be ≈0.5%. The low recombination efficiency means unbalance of charges (electrons and holes) in

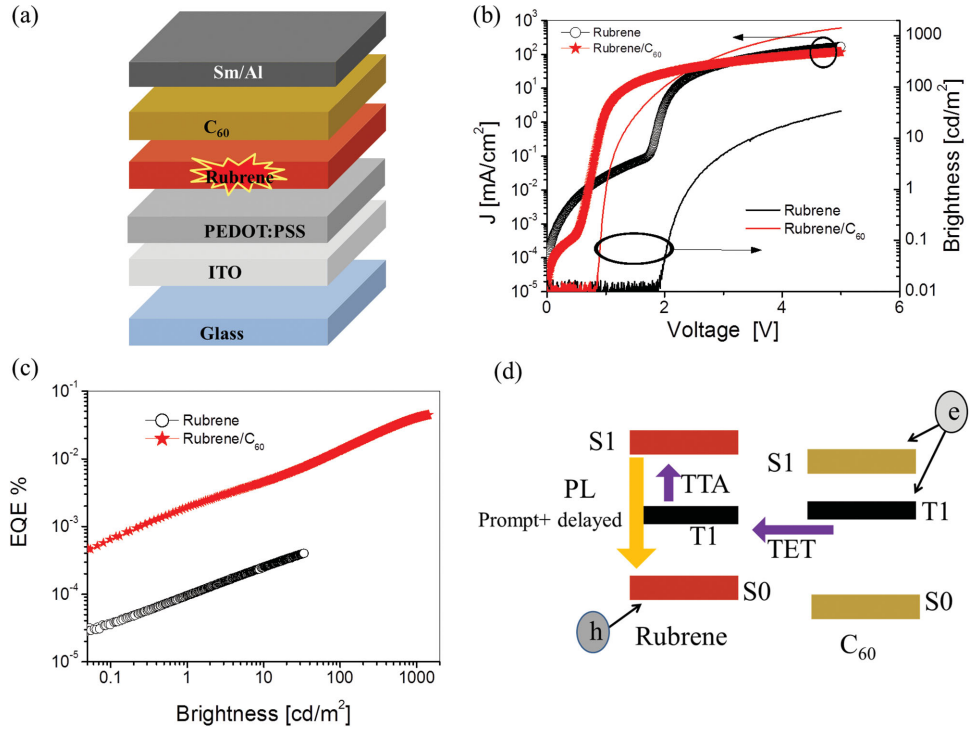

Figure 3. Electroluminescence from rubrene and rubrene/C_{60} OLEDs: a) device structure of a typical OLED with emissive layer of rubrene, an additional layer of C_{60} on top of rubrene was used to make the rubrene/C_{60} heterojunction device. b) *J–L–V* characteristics of rubrene and rubrene/C_{60} OLEDs. The rubrene/C_{60} OLED has an EL turn on of 1 V and produces two order of magnitude higher brightness at operating voltage of 5 V. c) EQE of rubrene and rubrene/C_{60} OLEDs. At same brightness, an order of magnitude higher EQE is measured for rubrene/C_{60} OLEDs. d) Physical model showing the contribution of TTA in overall light emission from rubrene, first externally injected electrons in the T1 of C_{60} are transferred to T1 in rubrene through CT-state-mediated TET; this is followed by efficient TTA in rubrene that generates extra singlets. The final emission therefore is a combination of prompt and delayed components. The suitably positioned T1 (1.12 eV) of rubrene assigns UC-EL operation at subgap operating voltages.

rubrene layer. Applying the same spin branching ratio (25%) for rubrene/C_{60} OLED, the estimated recombination efficiency values exceed 100%. This is a clear indication that extra singlets are being generated via TTA, and the classical spin branching ratio has changed. Assuming the ideal case scenario with 100% recombination efficiency in rubrene/C_{60} OLED, we estimate spin branching ratio of >26.4%. This observation establishes the positive influence of triplet states on EL in rubrene/C_{60} OLEDs. Now, assuming the TTA-induced maximum spin branching ratio of 62.5% (25% + 75%/2 = 62.5%), and PLQY of rubrene/C_{60} layer ≈ 0.075%, we estimate the maximum recombination efficiency of ≈43.5% in rubrene/C_{60} OLEDs. We note that C_{60} quench the PLQY of rubrene/C_{60} layer to ≈0.075%. (This value was calculated from measured PLQY of neat rubrene film and the average PL lifetime of rubrene and rubrene/C_{60} films). This result confirms that triplet excitons play an important role in EL generation. The emerging evidence of TTA in organic optoelectronics led us to ask the question—what would be the influence of triplet transfer from C_{60} on EL in integrated device platforms such as LEFETs? The role of triplets in EL is very topical as LEFETs are multifunctional devices, which integrate the functions of OLEDs and field effect transistors (FETs) into a single device architecture, thus offering a combination of emissive properties and logic functions.[16–27]

2.3. Recombination Efficiency in Rubrene/C_{60} Light-Emitting Transistors

In this section, we present the EL efficiency studies of rubrene/C_{60} heterojunction in LEFET device platform. Where applicable, the exact order of the heterojunction layer is reversed for the charge selective operation (n- or p-type) of LEFET devices.

Figure 4a shows a LEFET device architecture consisting of 400 nm thin composite layer of SiN_x capped with poly(methyl methacrylate) (PMMA) layer as gate dielectric, C_{60} as the n-type charge transporting layer, and rubrene as the light-emitting layer. The hole and electron injecting contacts were MoO_x/Au and Sm, respectively. Figure 4b shows the electrical transfer characteristics of the LEFET. The device shows excellent n-type transistor characteristics, negligible hysteresis, and high on/off ratio (>10^7). The electron mobility calculated from the transfer characteristics in saturation regime was 0.6 $cm^2\ V^{-1}\ s^{-1}$, which is similar to previously reported C_{60}-based transistors.[28–30] We note that this electron mobility is higher in comparison to the reported electron mobilities in LEFETs.[23–27]

The successful operation of C_{60}/rubrene LEFET is encouraging, but the key question is whether triplet excitons play a role in light emission from the LEFET. We have therefore measured the brightness and EQE of the LEFET operation. Figure 4b shows the electrical and optical transfer characteristics for C_{60}/rubrene LEFET. The brightness increases with the gate voltage and reaches up to 220 cd m^{-2} at V_g = 100 V. Figure 4c shows the electrical output characteristics of the LEFET, and EQE versus brightness is presented in Figure 4d. At the maximum brightness of 220 cd m^{-2} the measured EQE was 1.2×10^{-2}%. We note that in the context of LEFET operation (given that PLQY of rubrene is only 1.5%), this EQE value is very impressive. Assuming a spin branching ratio of 25%, we estimate that $\varphi_{capture} \approx 16.4\%$. This capture efficiency is higher as compared to recently reported similar structure LEFETs,[21,24,26,27]

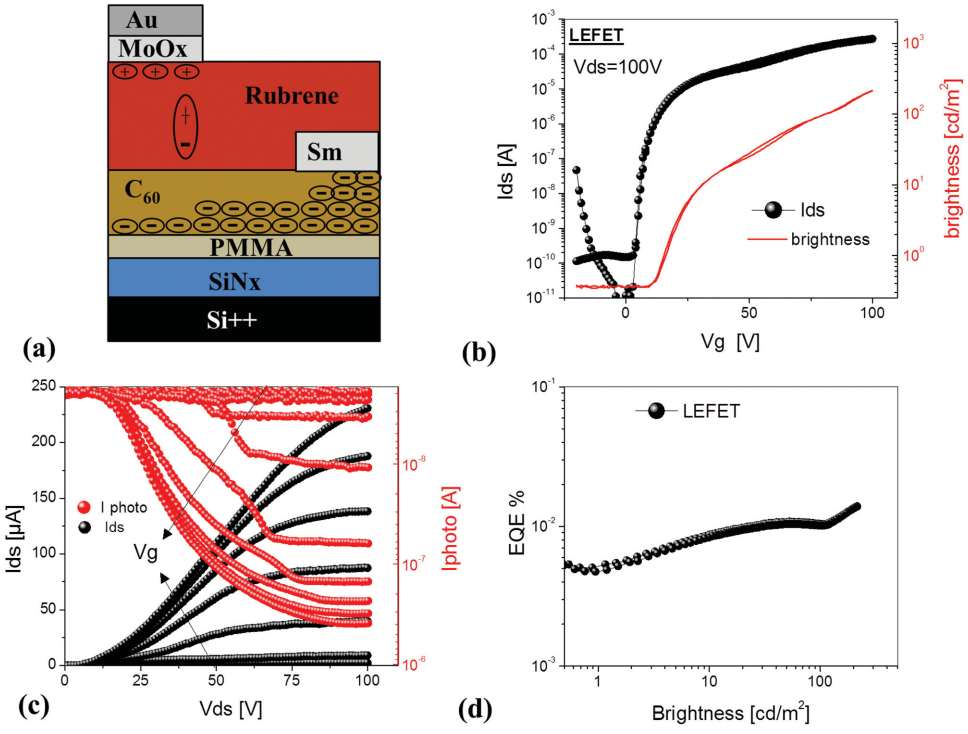

Figure 4. C_{60}/rubrene LEFET on a dielectric layer of SiNx/PMMA: a) schematics of device structure and operation of n-type LEFET using C_{60} as charge transport layer and the emissive layer of rubrene. b) Electrical and optical transfer characteristics of the LEFET. c) Electrical and optical output characteristics of the LEFET. d) EQE versus brightness of the C_{60}/rubrene LEFET.

Table 1. Summary of rubrene/C_{60} OLED and LEFET results.

Device parameters	Rubrene OLED	Rubrene/C_{60} OLED	C_{60}/Rubrene LEFET
μ_e cm^2 V^{-1} s^{-1}	–	–	0.6
μ_h cm^2 V^{-1} s^{-1}	–	–	–
On/off	–	–	>10^7
Max. brightness at 5 V [cd m^{-2}]	1450	435	220
EQE% at max. brightness	4×10^{-4}	4.5×10^{-2}	1.2×10^{-2}
Light-emitting area	20 mm^2	20 mm^2	0.048 mm^2 (3.10^{-3} mm × 16 mm)
Recombination efficiency ($\varphi_{capture}$)		43.5% (at spin branching of 62.5%)	6.6% (at spin branching of 62.5%) 16.4% (at spin branching of 25%)

thus indicative of enhanced recombination events of electron and holes. Now, assuming the TTA dominated modified spin branching ratio of 62.5%, we estimate $\varphi_{capture}$ to be at 4.6%, which is comparable to reported LEFET results (best reported values are ≈2%). In light of these results, we expect TTA to be influential in operation of C_{60}/rubrene LEFETs as well.

A closer look at the working mechanism of rubrene/C_{60} LEFET devices shown in Figure 4a indicates that electrons are injected from the source electrode (Sm; work function 2.7 eV) and move across the FET channel through the C_{60} layer (LUMO 4.3 eV) forming electron accumulation at the C_{60}/dielectric interface. The highest occupied-, lowest unoccupied-, molecular orbital (HOMO–LUMO) alignment is presented in Figure S5 (Supporting Information). The accumulated electrons are then transferred into the rubrene layer. Under the influence of the lateral source–drain electric field, holes are injected from the drain electrode (MoO_x/Au) into the HOMO of rubrene (5.4 eV).[10] These injected charges in rubrene and C_{60} progress through formation of CT excitons that eventually contribute in light emission. Akin to rubrene/C_{60} OLEDs discussed above, there are two possible routes for exciton formation. The first is direct exciton formation on the rubrene via electron injection from C_{60} and hole injection from MoO_x into rubrene. However, the barrier height for electron injection from C_{60} to rubrene is quite high (1.1 eV), which means this route is not efficient in light emission process. The second possibility is the exciton transfer from C_{60} to rubrene via TET route available at the C_{60}/rubrene interface.[10] As the triplet energy level of C_{60} (T1 = 1.56 eV) is higher than the triplet energy level of rubrene (T1 = 1.12 eV); this facilitates efficient triplet exciton transfer into the rubrene and light emission comes from TTA assisted recombination. Therefore, we assign TTA to be influential in light emission from C_{60}/rubrene LEFETs. A micrograph of light emission from the LEFET channel along with comparison of electroluminescence spectra from rubrene/C_{60} OLED and LEFET are given in Figure S6 (Supporting Information). Recombination efficiency at the maximum brightness is calculated in each case using Equation (1) and results for OLEDs and LEFET are given in **Table 1**.

2.4. Recombination Efficiency in p-Type Rubrene/C_{60} LEFETs

After analyzing the role of TTA in n-type C_{60}/rubrene LEFETs, we next studied its influence on EL efficiency in p-type rubrene/C_{60} LEFETs. For such p-type LEFETs, we used a solution processed poly(2,5-bis(3-hexadecylthiophen-2-yl)thieno[3,2-b]thiophene (PBTTT) layer. The PBTTT polymer is known for its high hole mobility as a charge transport layer.[21,26,27] **Figure 5**a,b shows p-type device architecture of LEFETs where modifications were applied to change the electron injection from the electron

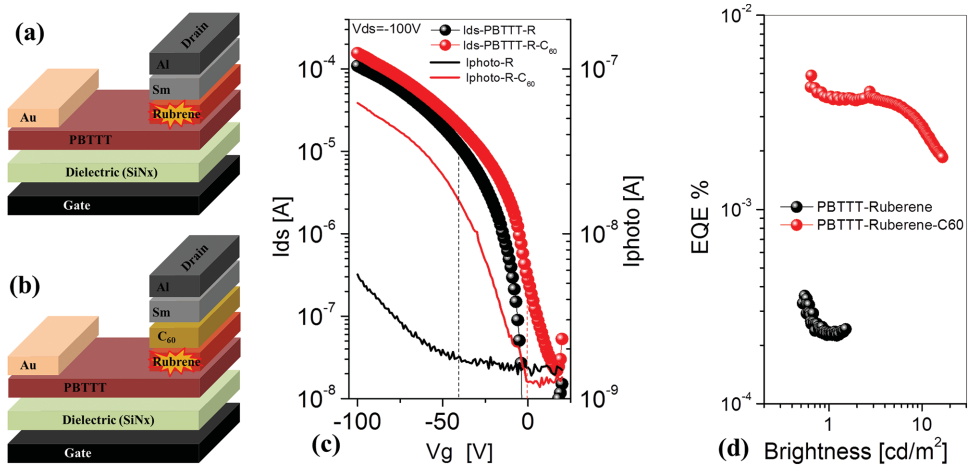

Figure 5. Modification of charge injection from the LEFET channel: a) shows the p-type LEFET device structure where charge injection from electron injecting electrode into the emissive layer of rubrene does not have a layer of C_{60}, hence works as a control device, b) electron injection modification by introduction of a thin layer of C_{60}. c) Optical and electrical characteristics of such p-type LEFETs produce high hole currents, mainly due to better transporting properties of PBTTT layer. d) EQE versus brightness of LEFETs where LEFET with C_{60} shows an order of higher magnitude EQE than the control LEFET.

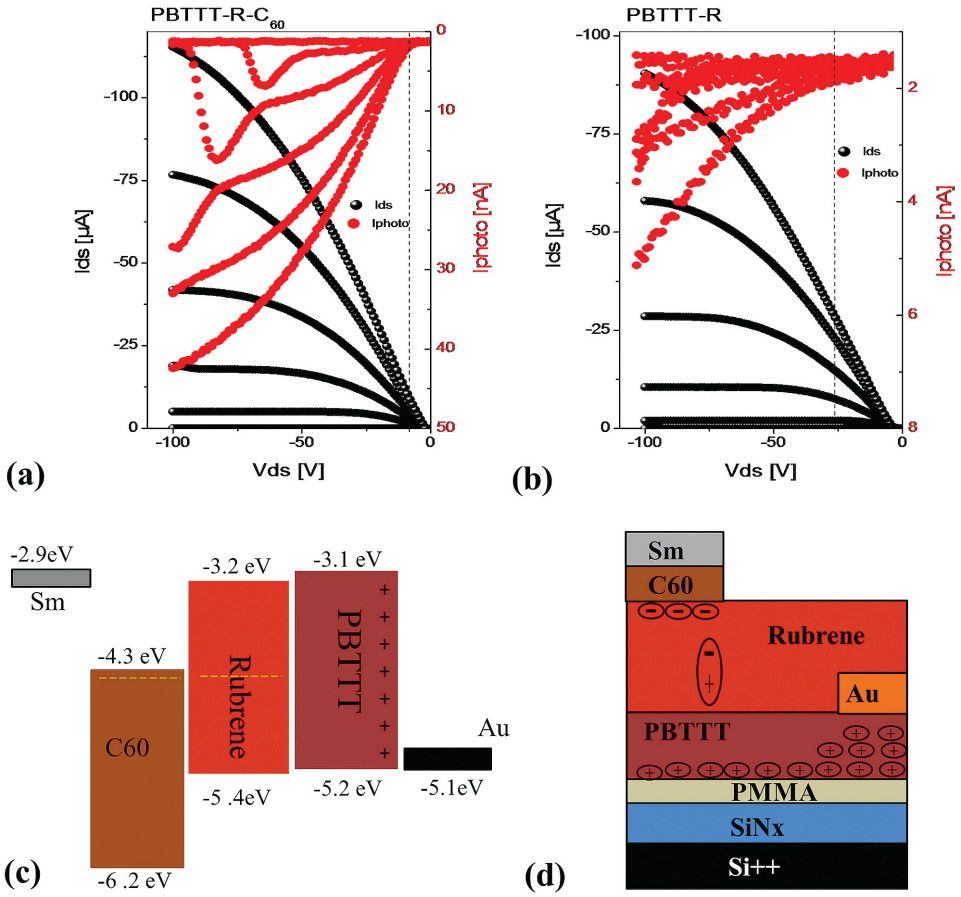

Figure 6. Output and optical characteristics of a) PBTTT/rubrene/C_{60} and b) PBTTT/rubrene LEFETs. The vertical line in output characteristics highlight the change in turn-on voltages; it is evident that the application of C_{60} produces brighter emission and lower turn-on voltages than the control PBTTT/rubrene LEFET. c) Schematics of HOMO–LUMO based energy level diagram of the multilayer LEFET structures. d) Charge injection and transport mechanism effective in LEFET operation of PBTTT/rubrene/C_{60}.

injecting metal contact into rubrene. The hole and electron injecting contacts were Au and Sm, respectively. For an insightful comparison of the potential role of C_{60} in light emission process, we introduced an additional layer of C_{60} under the Sm electrode, changing it to C_{60}/Sm. In this manner, electrons from Sm are not directly injected into rubrene but pass through the C_{60} interlayer.

The Figure 5c shows optical and electrical transfer characteristics of p-type LEFETs of PBTTT/rubrene with and without a C_{60} layer. An increase in turn-on voltage (and current) is observed in LEFETs without the C_{60} interlayer, as marked by broken vertical lines. To understand the light-emitting mechanism, we measured brightness and compare it with calculated EQE as a function of the gate voltage. Figure 5d clearly shows that the resulting EQE of LEFET devices with C_{60} is again higher than the control device of PBTTT/rubrene. It becomes apparent that C_{60} efficiently transfers triplets to rubrene and plays an important role in increasing the recombination efficiency and reducing the turn on voltages in p-type LEFETs. The detailed output characteristics (electrical and optical) of PBTTT/rubrene with and without C_{60} layer is shown in **Figure 6**a,b. The relevant energy level diagram and mechanism of device operation is shown in Figure 6c,d, respectively. Here, the holes are injected from the Au electrode into the PBTTT layer (HOMO 5.2 eV) and then subsequently transferred to HOMO of rubrene. The electrons are directly injected from the Sm electrode in the lowest unoccupied molecular orbital (LUMO) of rubrene. The p-type devices showed excellent p-channel transistor characteristics, and high on/off ratio (>10^5). The hole mobility of LEFET with C_{60} was 0.07 $cm^2\ V^{-1}\ s^{-1}$. The control device showed similar mobility (0.05 $cm^2\ V^{-1}\ s^{-1}$), meaning C_{60} layer did not alter the electrical characteristics. A summary of the results for modified LEFET devices is given in **Table 2**.

As evident from results presented in Table 1 and Table 2, we consistently observe an improved EQE for light emission from the rubrene layer whenever a layer of C_{60} is used. In combination with the spectroscopic evidence, and the presented energy UC-EL effect in rubrene/C_{60} OLEDs, it becomes apparent that charge injection into the C_{60} layer and subsequent transfer of excitons to rubrene plays an important role in increasing the spin branching ratio above 25%. The heterojunction devices consistently produce higher charge recombination efficiencies.

3. Conclusions

In summary, we have shown a new process of charge recombination that is effective in increasing the emission efficiency of

Table 2. Summary of rubrene/C_{60} LEFET results with p-type charge-transporting layer of PBTTT.

Device	Emissive layer composition	EQE [%]	Turn-on voltage [V]
PBTTT–LEFET	Rubrene–C_{60}	0.0035	–5
		($\varphi_{capture}$ = 1.9% at spin branching of 62.5%)	
		($\varphi_{capture}$ = 4.8% at spin branching of 25%)	
	Rubrene	0.00023	–25
		($\varphi_{capture}$ = 0.31% at spin branching of 25%)	

OLEDs and LEFETs. Using the model heterojunction of rubrene/C_{60}, we show that triplet excitons contribute in generating extra singlets via the TTA route. Ultrafast TA measurements confirm two independent routes of triplet formation in rubrene/C_{60} films. In addition to direct singlet fission from upper excited singlet state in rubrene triplet excitons density increases via the ^{3}CT-state-mediated TET to T1 in rubrene. The CT-state-mediated TET process from C_{60} to rubrene makes TTA a very efficient process and its influence is recognized in EL turn-on at subgap voltages in OLEDs, and high recombination efficiencies in LEFETs.

4. Experimental Section

Spectroscopy: TCSPC measurements were undertaken using a time-resolved fluorescence spectrometer (Halcyone, Ultrafast Systems) operating in TCSPC mode. An amplified Ti:sapphire laser system (Spitfire ACE, Spectra Physics) was used as the excitation source, delivering ≈100 fs laser pulses at 800 nm with a 1 kHz repetition rate. ≈150 μJ of the laser output was attenuated and used as a time-to-amplitude converter stop signal, and the remainder of the laser fundamental was coupled to an optical parameter amplifier (OPA) system (Topas Prime, Light Conversion) delivering fs tunable excitation pulses at 470 nm. Thin film samples were mounted inside a custom built optical chamber filled with inert (N_2) gas, and PL decay profiles were monitored at 570 nm after passage through a single grating monochromator. Two set of thin film samples grown on fused silica substrates with rubrene layer thickness ranging from 35 to 50 nm with or without a 25 nm layer of C_{60} were investigated. Steady state PL spectra were recorded at 470 nm excitation using Fluoromax-4 spectrophotometer, a Cary 5000 spectrometer was used for recording the UV–vis spectra.

For TA, the same amplified laser system was used as the excitation source, and measurements were undertaken using a broadband pump–probe TA spectrometer (Helios, Ultrafast Systems). ≈50 μJ of the laser output was attenuated and focused onto a 3 mm sapphire window to generate a white light continuum probe pulse in the visible region from 430 to 730 nm. Thin film samples were mounted inside the same custom built optical chamber filled with inert (N_2) gas, and had an absorbance of ≈0.2 at the excitation wavelength of 470 nm. The instrument response function had a full width at half maximum of ≈200 fs, measured experimentally by a Gaussian fit to the scattered laser excitation profile. All spectra were corrected for the chirp of the probe pulses, and the resulting time traces were analyzed globally using commercially available software (Igor, Version 6.1.2.1, Wavemetrics).

OLED and LEFET Devices: OLEDs consisting of rubrene as the emissive layer were fabricated on precleaned indium tin oxide (ITO) layer on glass substrates. A 25 nm thin layer of poly(ethylenedioxythiophene):polystyrene sulfonate (PEDOT:PSS) was spin coated on ITO before sublimation of 25 nm rubrene in vacuum at a base pressure of 2×10^{-6} mbar. A 25 nm thin layer of C_{60} was deposited separately for rubrene/C_{60} heterojunction OLEDs. A 1 nm thin Sm and 80 nm thin Al layer were evaporated through shadow masks as top electrode. All OLED devices have an active area of 20 mm^2. The electrical characteristics reported are average of at least 12 devices.

All LEFETs were fabricated using a heavily n-doped Si wafers with a 400 nm SiN*x*, which were purchased from Silicon Quest International, Inc. These wafers were precisely diced and cleaned in a Class 1000 clean room by ultrasonication in isopropanol followed by acetone. The rest of the fabrication and testing was performed inside a nitrogen glovebox (O_2 and H_2O levels <0.1 ppm). An additional 150 nm thick dielectric passivation layer of PMMA (120 000 g mol^{-1}) was spin-coated onto the SiN_x substrates. After spin-coating, substrates were annealed on a hot plate at 150 °C for 30 min. Film thicknesses were measured using a Dektak 150 profilometer. A 50 nm layer of C_{60} was deposited on top of the PMMA layer by thermal evaporation followed by a 35 nm layer of rubrene film, in high vacuum (3×10^{-6} mbar). Interdigitated source and drain contacts were formed by vacuum evaporation of MoO_x/Au and Sm using two shadow masks as described in previous reports.[20]

All OLED and LEFET devices were characterized using an Agilent B1500A semiconductor device analyzer and an SA-6 Semiauto probe station with a calibrated photomultiplier tube (PMT) positioned over the device. The source–drain current in the transistor channel and photocurrent in the PMT were recorded to determine the device parameters. Electrical and optical characteristic parameters of the devices were calculated using the reported method assuming Lambertian emission from the device.[22] Solid-state PLQY measurements of rubrene were obtained from evaporated films on glass according to the reported methodology.[31]

Supporting Information

Supporting Information is available from the Wiley Online Library or from the author.

Acknowledgements

A.K.P. acknowledges support from the University of Queensland–NSRSG award and Australian Renewable Energy Agency fellowship award (Project 06-F022). E.G.M. acknowledges financial support by the Australian Research Ccouncil (FT100100795). E.B.N. is a receipient of an Australian Research Council Future Fellowship (FT110100216). Ultrafast measurements were undertaken at the Photochemistry and Ultrafast Laser Spectroscopy (PULSE) facility, School of Chemistry and Molecular Biosciences, established with financial support by the University of Queensland (MEI-2013000106). This work was performed in part at the Queensland node of the Australian National Fabrication Facility (ANFF)—a company established under the National Collaborative Research Infrastructure Strategy to provide nano- and microfabrication facilities for Australia's researchers.

Received: July 15, 2015
Revised: September 9, 2015
Published online:

[1] M. Pope, C. Swenberg, *Electronic Processes in Organic Crystals*, Oxford University Press, Oxford **1982**.
[2] C. W. Tang, S. A. VanSlyke, *Appl. Phys. Lett.* **1987**, *51*, 913.
[3] M. A. Baldo, D. F. O'Brien, Y. You, A. Shoustikov, S. Sibley, M. E. Thompson, S. R. Forrest, *Nature* **1998**, *395*, 151.

[4] J. Shinar, R. Shinar, *J. Phys. D: Appl. Phys.* **2008**, *41*, 133001.
[5] H. Yersin, A. F. Rausch, R. Czerwieniec, T. Hofbeck, T. Fischer, *Coord. Chem. Rev.* **2011**, *255*, 2622.
[6] H. Uoyama, K. Goushi, K. Shizu, H. Nomura, C. Adachi, *Nature* **2012**, *492*, 234.
[7] D. Y. Kondakov, T. D. Pawlik, T. K. Hatwar, J. P. Spindler, *J. Appl. Phys.* **2009**, *106*, 124510.
[8] M. B. Smith, J. Michl, *Chem. Rev.* **2010**, *110*, 6891.
[9] G. B. Piland, J. J. Burdett, R. J. Dillon, C. J. Bardeen, *J. Phys. Chem. Lett.* **2014**, *5*, 2312.
[10] A. K. Pandey, *Sci. Rep.* **2015**, *5*, 7787.
[11] G. B. Piland, J. J. Burdett, D. Kurunthu, Christopher J. Bardeen, *J. Phys. Chem. C* **2013**, *117*, 1224.
[12] L. Ma, K. Zhang, C. Kloc, H. Sun, M. E. Michel-Beyerle, G. G. Gurzadyan, *Phys. Chem. Chem. Phys.* **2012**, *14*, 8307.
[13] V. Jankus, E. W. Snedden, D. W. Bright, E. Arac, D. C. Dai, A. P. Monkman, *Phys. Rev. B* **2013**, *87*, 224202.
[14] A. K. Pandey, J.-M. Nunzi, *Adv. Mater.* **2007**, *19*, 3613.
[15] D. Y. Kondakov, *Philos. Trans. R. Soc. A* **2015**, *373*, 20140321.
[16] A. Hepp, H. Heil, W. Weise, M. Ahles, R. Schmechel, He. von Seggern, *Phys. Rev. Lett.* **2003**, *91*, 157406.
[17] M. A. McCarthy, B. Liu, E. P. Donoghue, I. Kravchenko, D. Y. Kim, F. So, A. G. Rinzler, *Science* **2011**, *332*, 570.
[18] K. Nakamura, T. Hata, A. Yoshizawa, K. Obata, H. Endo, K. Kudo, *Jpn. J. Appl. Phys.* **2008**, *47*, 1889.
[19] M. Ullah, K. Tandy, Soniya D. Yambem, K. Muhieddine, P. Meredith, P. Burn, Ebinazar B. Namdas, *Org. Electron.* **2015**, *17*, 371.
[20] E. B. Namdas, P. Ledochowitsch, J. D. Yuen, D. Moses, A. J. Heeger, *Appl. Phys. Lett.* **2008**, *92*, 183304.
[21] B. B. Y. Hsu, J. Seifter, C. J. Takacs, C. Zhong, H.-R. Tseng, I. D. W. Samuel, E. B. Namdas, G. C. Bazan, F. Huang, Y. Cao, A. J. Heeger, *ACS Nano* **2013**, *7*, 2344.
[22] M. Ullah, K. Tandy, J. Li, Z. Shi, P. L. Burn, P. Meredith, E. B. Namdas. *ACS Photonics* **2014**, *1*, 954.
[23] R. Capelli, S. Toffanin, G. Generali, H. Usta, A. Facchetti, M. Muccini, *Nat. Mater.* **2010**, *9*, 496.
[24] M. Ullah, K. Tandy, S. D. Yambem, M. Aljada, P. L. Burn, P. Meredith, E. B. Namdas, *Adv. Mater.* **2013**, *25*, 6213.
[25] K. Tandy, M. Ullah, P. L. Burn, P. Meredith, E. B. Namdas. *Org. Electron.* **2013**, *14*, 2953.
[26] M. C. Gwinner, S. Khodabakhsh, M. H. Song, H. Schweizer, H. Giessen, H. Sirringhaus, *Adv. Funct. Mater.* **2009**, *19*, 1360.
[27] J. Zaumseil, R. H. Friend, H. Sirringhaus, *Nat. Mater.* **2006**, *5*, 69.
[28] G. Schwabegger, M. Ullah, M. Irimia-Vladu, M. Reisinger, Y. Kanbur, R. Ahmed, P. Stadler, S. Bauer, N. S. Sariciftci, H. Sitter. *Synth. Met.* **2011**, *161*, 2058.
[29] M. Ullah, T. B. Singh, H. Sitter, N. S. Sariciftci. *Appl. Phys. A: Mater. Sci. Process* **2009**, *97*, 521.
[30] M. Ullah, I. I. Fishchuk, A. K. Kadashchuk, P. Stadler, A. Pivrikas, C. Simbrunner, V. N. Poroshin, N. S. Sariciftci, H. Sitter. *Appl. Phys. Lett.* **2010**, *96*, 213306.
[31] N. C. Greenham, I. D. W. Samuel, G. R. Hayes, R. T. Phillips, Y. A. R. R. Kessener, S. C. Moratti, A. B. Holmes, R. H. Friend, *Chem. Phys. Lett.* **1995**, *241*, 89.